

Operational modal analysis on a wind turbine blade

F. Marulo¹, G. Petrone¹, V. D'Alessandro¹, E. Di Lorenzo^{1,2}

¹University of Naples "Federico II", Department of Industrial Engineering,
Via Claudio 21, 80125, Naples, Italy
e-mail: francesco.marulo@unina.it

²LMS, A Siemens Business, RTD Test Division,
Interleuvenlaan 68, 3001, Leuven, Belgium

Abstract

The structural integrity of blades is critical in order to allow the operation of a wind turbine. An appropriate knowledge about their dynamic characteristics is desired in early design stages too. The effect of some local failure on the modal parameters of a wind turbine blade is experimentally investigated. The investigated wind turbine blade is 6.4 m long and is made of glass fibers combined with epoxy resin. During the tests, the blade is assumed to be clamped at the root. In order to identify the effect of some failures on the modal parameters, the experimental campaign is divided in several steps: (i) an operational modal analysis to extract the modal parameters before the failure; (ii) a static test, in which the blade exhibits one or more failures; (iii) another operational modal analysis on the damaged structure. Experimental results reveal a decrease in the natural frequencies and an increase of the estimated modal damping of the structure. The reduction in natural frequencies is a result of a decrease of the stiffness of the structure because of some structural failures.

1 Introduction

Performing modal tests on large structures such as wind turbines, buildings, bridges and airplanes is a challenging task. The problem is not in measuring the responses, but in exciting the structures. Wind turbines are huge and flexible structures with aerodynamic and gravitational forces acting on the rotating blades. Excessive structural vibrations have always been a design concern. Output-only modal analysis has been developed, in its first attempt, for determining the modal parameters of a wind turbine. It was called Natural Excitation Testing (NExT), rather than Operational Modal Analysis (OMA). A critical step in the development of NExT was to find a function that could be measured from operational data and that possessed a clear relationship with the modal parameters of the structure [1]. The selected function was the so called cross-correlation between responses without a measurement of the input forces. The NExT procedure was a predecessor to the commonly used OMA techniques. Although the first application of an OMA methodology was related to a vertical-axis wind turbine, not many other applications to wind turbines were studied later on. The main reason is the fact that most of the OMA assumptions are violated by operating wind turbines.

The structural integrity of blades is critical in order to allow the operation of a wind turbine. Modal parameters are directly influenced by the physical properties of the structure. So, any change in the physical properties should cause a change in its modal parameters and it can be used for Structural Health Monitoring (SHM) purposes. A SHM technique should be implemented for on-line continuous monitoring of wind turbines by comparing the differences between the monitored modal parameters and their baseline values. A warning level would indicate when the blades are going toward a physical damage.

2 Geometry and materials

2.1 Geometry

The investigated structure is a 6.5 meter all fiberglass blade from a 30 kW wind turbine. Two airfoils were used for the blade sections: the first with a maximum thickness of 25% used from the root up to 27% of the radius, and the second blade with a maximum thickness of 21% used by 30% up to the end. The two airfoils were combined with a connection one.

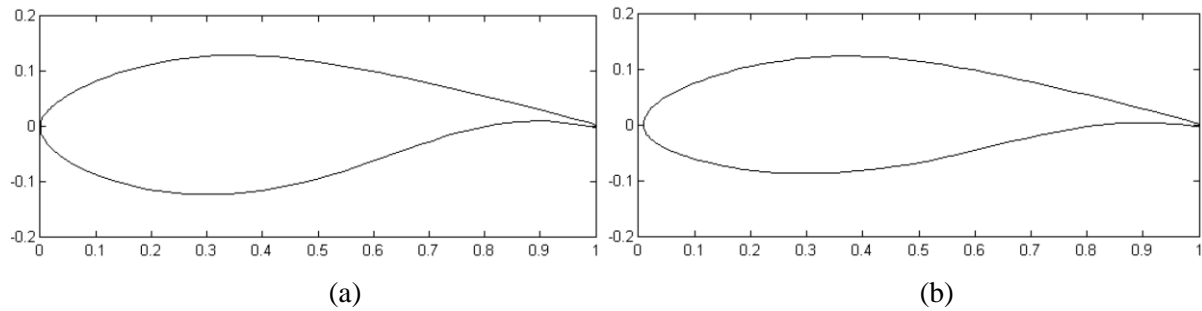


Figure 1: Geometries of the airfoils with 25% (a) and 21% (b) as maximum thickness.

Chord and twist distribution was obtained by means of an optimization code in which the maximum area was fixed and the requirement was the nominal rotation speed of 80 rpm. The main geometrical parameters are reported in Figure 2a while from Figure 2b it has to be noted the reduced section of the free edge in order to reduce the aerodynamic noise.

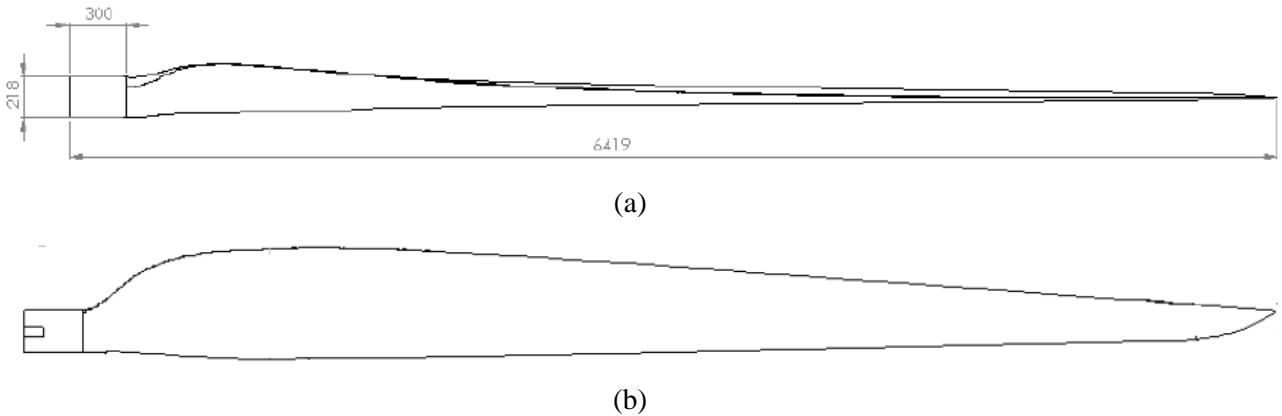


Figure 2: Views of the blade.

2.2 Materials

The wind turbine blade is made of a high performance foam core (DIAB Divinycell H45), offering excellent mechanical properties to low weight, arising from the combination of polyurea and pvc, covered by fibreglass composites. The material properties of the core are listed in Table 1.

Two different configurations of glassfibres laminates were used: unidirectional and fabric. The material properties of both the configurations, carried out by static test according to the ASTM standards and

indicated with the subscript 1 the longitudinal direction and the subscript 2 the transversal one, are listed in Table 2.

	Young's modulus E [GPa]	Shear modulus G [GPa]	Poisson's ratio ν	Mass density ρ [kg/m ³]
Foam H 45	59.0	15.9	0.32	48

Table 1: Core mechanical properties.

Different configurations of the composite material (stacking sequence, number of plies) are distributed along the blade span. In Figure 3 the different material configurations are shown by using different colours.

	Longitudinal Young's modulus E_1 [GPa]	Transversal Young's modulus E_2 [GPa]	Shear modulus G_{12} [GPa]	Poisson's ratio ν	Mass density ρ [kg/m ³]
unidirectional	30.0	7.0	4.0	0.22	2200
Fabric	15.6	15.6	4.0	0.27	2200

Table 2: Laminates mechanical properties.

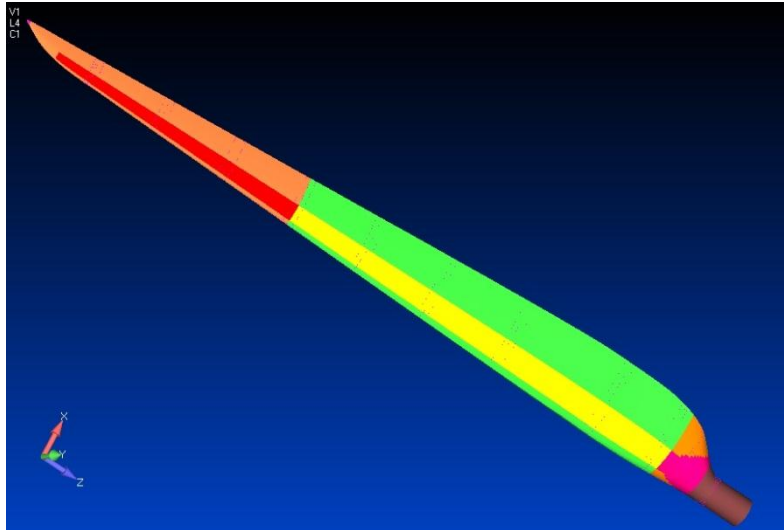


Figure 3: Material distribution along the blade.

3 Experimental investigation

3.1 Operational Modal Analysis (OMA)

Operational Modal Analysis (OMA) technique allows extracting the modal parameters from vibration response signal by means of auto and cross- correlations functions. The main difference compared to the

traditional experimental modal analysis is that it does not need the measurement of the input forces. Structures under operating conditions or in situations where it is impossible to measure the input forces can be tested. The information obtained by means of OMA can be used for several purposes such as the improvement of numerical models, the prediction of the dynamic behavior of new designs, the identification of the modal parameters of prototypes and the monitoring of systems in operating conditions in order to predict in advance possible failures or damages.

It is possible to extend common identification methods to situations in which the input forces cannot be measured. The system must comply with three main assumptions. It must be Linear Time Invariant, the excitation forces must be represented by a flat white noise spectrum in the band of interest and they have to be uncorrelated. The better these assumptions are fulfilled, the better the quality of the estimated modal parameters.

3.1.1 Operational Polymax

Several OMA techniques have been developed and evaluated in the past years. In this paper, the Polymax method [2] has been selected to perform the operational modal analysis. It has been developed as a polyreference version of the least-squares complex frequency-domain (LSCF) estimation method using a so-called right matrix-fraction model. In case of Experimental Modal Analysis (EMA), the modal decomposition of an FRF matrix $[H(\omega)]$ is described in Equation (1):

$$[H(\omega)] = \sum_{i=1}^M \frac{\{v_i\} \langle l_i^T \rangle}{j\omega - \lambda_i} + \frac{\{v_i^*\} \langle l_i^H \rangle}{j\omega - \lambda_i^*} \quad (1)$$

where l is the number of outputs; M is the number of modes, $*$ is the complex conjugate operator, H is the complex conjugate transpose of a matrix, $\{v_i\}$ are the mode shapes, are the modal participation factors and λ_i are the poles.

The relationship that occurs between poles, eigenfrequencies ω_i and damping ratios ξ_i is:

$$\lambda_i \lambda_i^* = -\xi_i \omega_i \pm j\sqrt{1 - \xi_i^2} \omega_i \quad (2)$$

The input spectra $[S_{uu}(\omega)]$ and output spectra $[S_{yy}(\omega)]$ of a system represented by the FRF matrix are related as:

$$[S_{yy}(\omega)] = [H(\omega)] [S_{uu}(\omega)] [H(\omega)]^H \quad (3)$$

Unlike in EMA, where FRFs between input and outputs are used, OMA uses output-only data. A leakage-free and Hanning-window free pre-processing method is used to estimate the power and cross spectra. The weighted correlogram approach was adopted: correlations with positive time lags are computed from the time data; an exponential window is applied to reduce leakage and the influence of the noisier higher time lag correlation samples; and finally the DFT of the windowed correlation samples is taken. An exponential window is compatible with the modal model and therefore, the pole estimates can be corrected for the application of such a window. More details about this pre-processing and the comparison with the more classical Welch's averaged periodogram estimate (involving Hanning windows) can be found in [3].

The Polymax algorithm greatly facilitates the operational modal parameter estimation process by producing extremely clear stabilization diagrams, making the pole selection a lot easier by means of estimating unstable poles (i.e. mathematical or noise modes) with negative damping making them relatively easy to separate from the stable poles (i.e. system modes) [2, 3].

3.1.2 Stochastic subspace identification

Another advanced OMA method is the Stochastic Subspace Identification (SSI) one. The term subspace means that the method identifies a state-space model and that it involves a Singular Value Decomposition

(SVD) truncation step. There are several variants in this class of methods including Canonical Variate Analysis (CVA) and Balanced Realization (BR).

In this method a so-called stochastic state space model is identified from output correlations or directly from measured output data [7]. The state space model is written in Equation (5):

$$\begin{aligned} x_{k+1} &= Ax_k + w_k \\ y_k &= Cx_k + v_k \end{aligned} \quad (4)$$

where y_k is the sampled output vector, x_k is the discrete state vector, w_k is the process noise due to disturbances and unknown excitation of the structure, v_k is the measurement noise, mainly due to sensor inaccuracy, but also to the unknown excitation of the structure; k is the time instant. The matrix A is the state transition matrix that completely describes the dynamics of the system by its eigenvalues; C is the output matrix. The only known terms in Equation (5) are the output measurements y_k and the challenge is to determine the system matrices A , C from which the modal parameters can be derived.

The derivation of the modal parameters starts with the eigenvalue decomposition of A :

$$A = \Psi \Lambda_d \Psi^{-1} \quad (5)$$

where Ψ is the eigenvector matrix and Λ_d is a diagonal matrix containing the discrete-time eigenvalues μ_i which are related to the continuous-time eigenvalues λ_i as:

$$\mu_i = \exp(\lambda_i \Delta t) \quad (6)$$

The eigenfrequencies and damping ratios are related to λ_i as expressed in Equation (2). Finally, the mode shapes are found as:

$$V = C\Psi \quad (7)$$

3.2 Experimental setup

The dynamic characteristics of the wind turbine blade are determined through operational modal analysis (OMA). Two tests were performed, one before and another one post buckling, in order to investigate the influence of a damage on the modal parameters. In Figure 4 the sketch of the experimental setup is shown. The wind turbine blade under investigation was fixed to a rigid structure at only one end, resulting as a cantilever beam, and on the opposite free end it was artificially excited by hands.



Figure 4: Sketch of the experimental OMA set-up.

The responses were recorded by using ten uni-axial accelerometers (PCB 352B10) located in two rows on five sections along the blade in order to evaluate both flexural and torsional mode shapes. The accelerometers were connected to the acquisition system LMS SCADAS III, which was connected to a computer for the recording of the data. The whole acquisition process was controlled through the software LMS Test.Lab, which is able to display, in real time, the Frequency Response Function of the excited node on the experimental mesh. Vibration measurements were taken in the frequency range 0-256 Hz. Once the experimental test was concluded, modal parameters were extracted through PolyMAX algorithm and SSI method, both of them available again in LMS Test.Lab.

3.3 Experimental results

The global dynamic responses of the wind turbine blade pre and post buckling were measured and the autopowers at a tip node in the out-of-plane direction are represented in Figure 5.

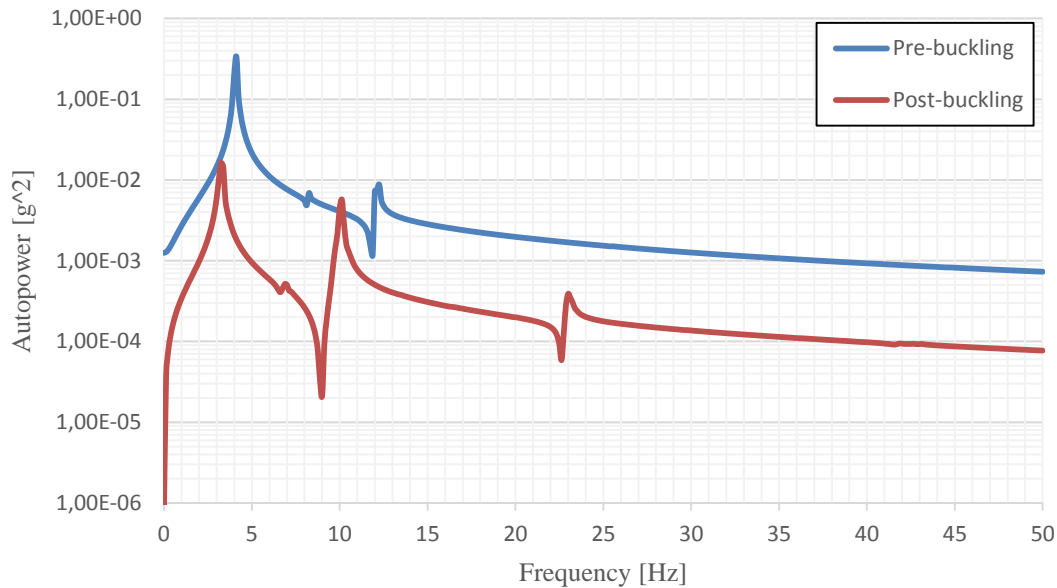


Figure 5: Autopowers pre and post buckling at a tip node in out-of-plane direction.

From Figure 5 it is possible to highlight that there is a shift of the natural frequencies for the “damaged” model with respect to the “undamaged” one. This should be evident since damages can be seen as a reduction of the material properties and, consequently, of the stiffness of the structure that is directly dependent with natural frequencies. Furthermore it is difficult to identify all the natural frequencies by looking at the spectrum of the crosscorrelations. However a comparison of the first four modes, obtained with two different techniques, is reported in Table 3.

Table 3 shows the comparison between the two set of modal parameters by applying the two different techniques explained in Section 3.1. Concerning the natural frequencies, a good agreement has been found. More uncertainties are related to the damping ratios. The main differences can be seen in the estimation of the damping for the second mode both for pre and post buckling conditions.

Figure 6 and Figure 7 show, respectively, the stabilization diagram obtained by using Polymax (left) and SSI (right) fitting models of increasing orders (from 2 to 40) to the spectra. Poles are then selected and mode shapes evaluate.

Mode n.	Pre buckling				Post buckling			
	Natural frequency [Hz]		Damping ratio (%)		Natural frequency [Hz]		Damping ratio (%)	
	Polymax	SSI	Polymax	SSI	Polymax	SSI	Polymax	SSI
1	3.93	3.91	2.06	2.48	3.19	3.24	1.98	1.79
2	7.92	7.95	0.74	1.24	6.09	6.22	2.90	3.71
3	11.33	11.42	1.35	1.08	9.98	9.96	1.01	0.71
4	24.78	24.78	0.65	0.71	22.93	23.09	0.47	0.55

Table 3: Modal parameters of the investigated blade pre and post buckling. Comparison between the two techniques (Polymax, SSI).

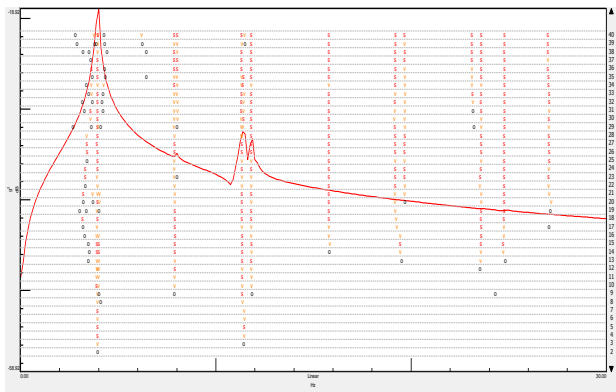


Figure 6 – Polymax: Stabilization diagram

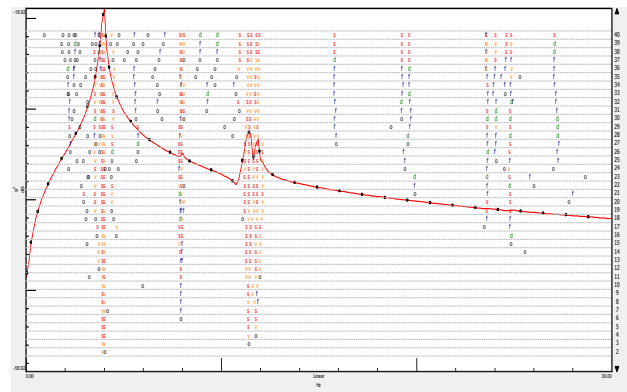


Figure 7 – SSI: Stabilization diagram.

As can be seen, by using Polymax the stabilization diagram is very clear, with column of stable poles that can be easily identified. Also the synthesis of the spectra with the identified modal model shows a good correlation with those calculated from the time data series both in pre and post buckling conditions, as can be seen in Figure 8. By using the SSI technique the stabilization diagram is less clear mainly around the first natural frequency, but finally the obtained modal parameters are very similar to the ones obtained by using Polymax.

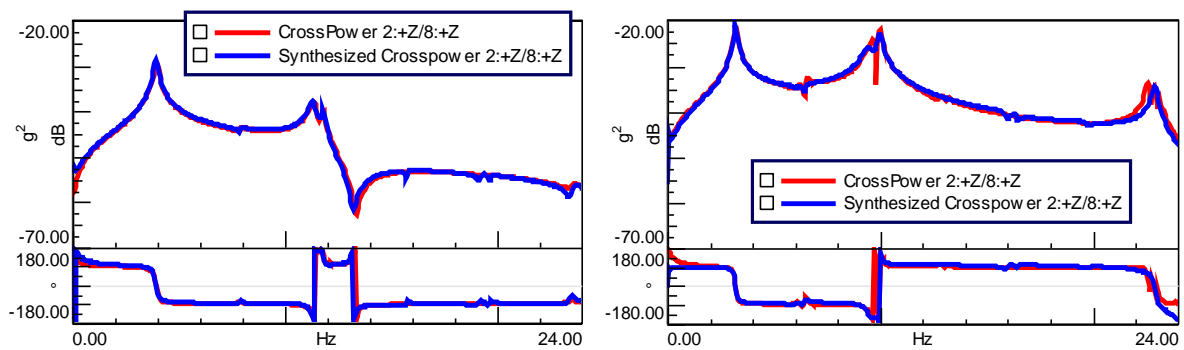


Figure 8 – Original and synthesized crosspowers for the same measurement point for the pre-bucking condition (left) and the post-bucking condition (right).

4 Numerical investigation

A finite element analysis (FEA) of the blade was modelled using 4-nodes quadrilateral elements (CQUAD4) for the skins of the blade and rigid elements (RBE3). The numerical mesh consisted of 11805 nodes and 10867 elements.

The modal analysis is carried out using the commercial finite element solver MSC/Nastran 2008. Moreover, in order to compare the experimental and numerical Frequency Response Function (FRFs), a unit force is applied on the node of one corner of the upper face of the blade, and prediction of the accelerations as a function of the frequency is accomplished on different points. An isometric view of the FE model is shown in Figure 9.

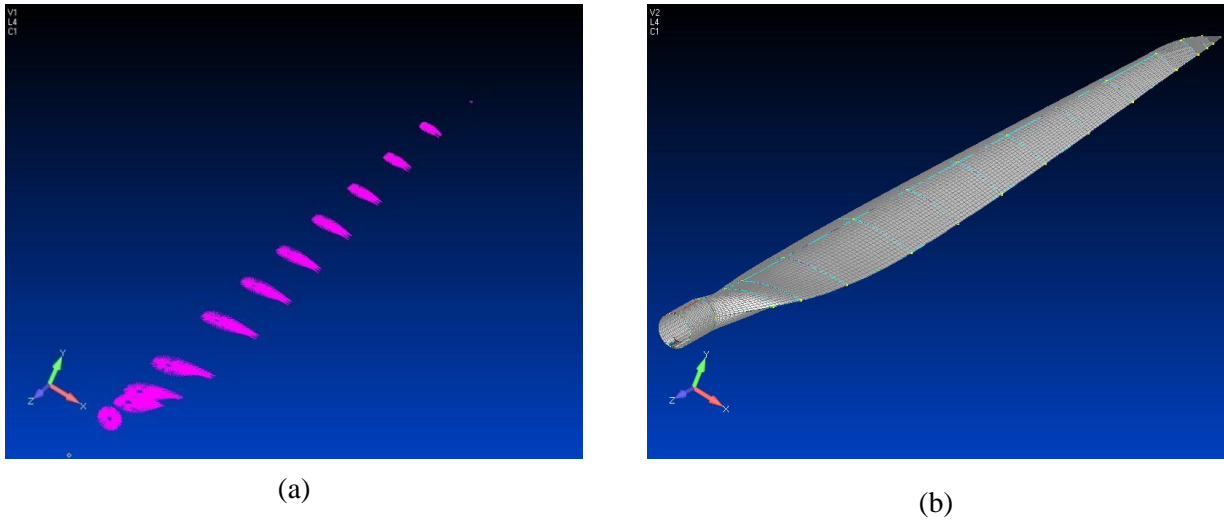


Figure 9: Isometric view of FE model: rigid (a) and 4-nodes quadrilateral (b) elements.

4.1 Numerical results

Numerical results, in terms of natural frequencies and mode shapes, were obtained. The results show that the 1st and the 3th eigenmodes are the fundamental flapwise bending modes while the 2nd and the 4th eigenmodes are the edgewise bending modes. The first four mode shapes are presented in Figure 10.

4.2 Linear buckling analysis

A linear buckling analysis of the 3D FE model was conducted by subjecting the blade to the loading condition of maximum tip displacement. This analysis is used for designing secondary structural elements, such as the skin core thickness. In particular the idea is to increase the skin core thickness of a region where buckling occurs by an amount proportional to the exceed quantity of the constraint condition $\lambda \leq 1$, where λ is the buckling eigenvalue associated with the applied load. The inclusion of this effect in the design process is important because the distribution of secondary structural material has a significant influence on the non-structural mass, which in turn affects the dynamic behavior of the blade by changing its natural frequencies. The first buckling mode is shown in Figure 11. It is localized in the sections near the blade root and it is higher than 1 and so it is not critical for the applied loading condition (i.e. $\lambda \leq 1$).

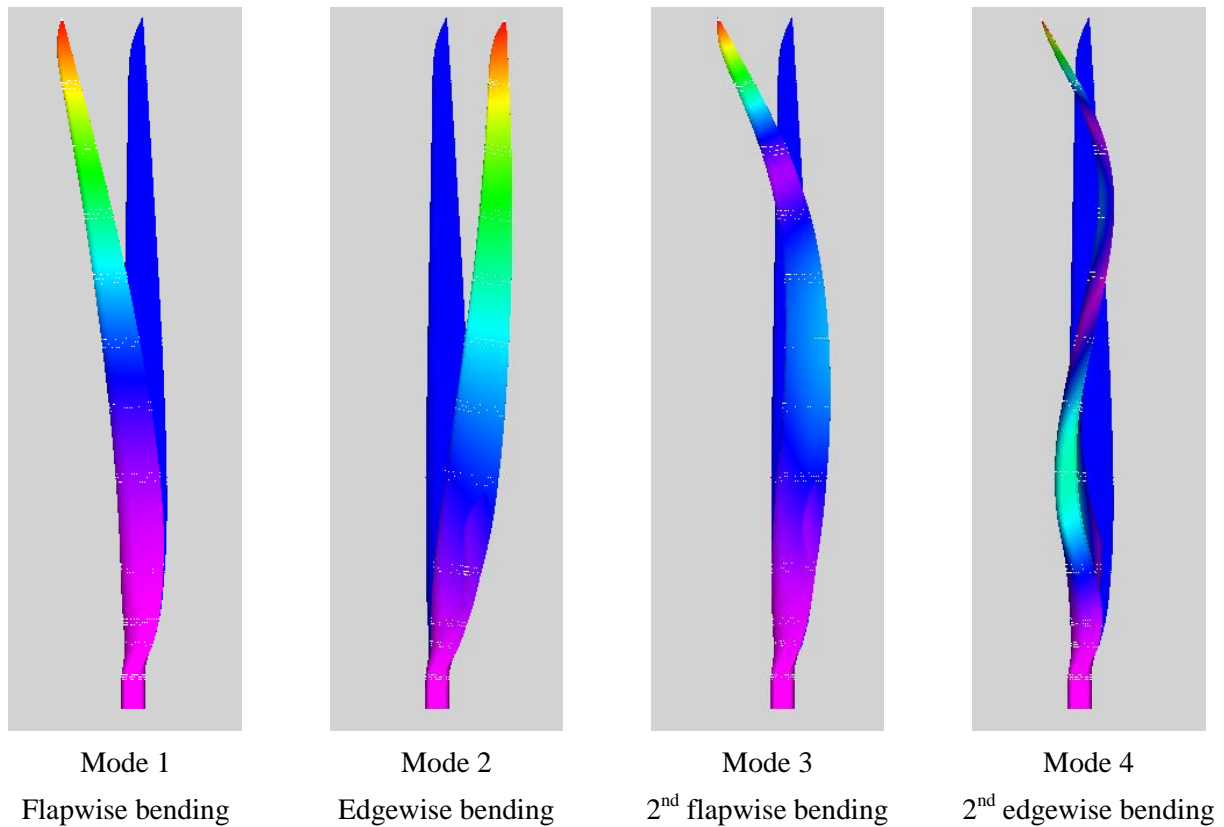


Figure 10: First four mode shapes of the wing turbine.

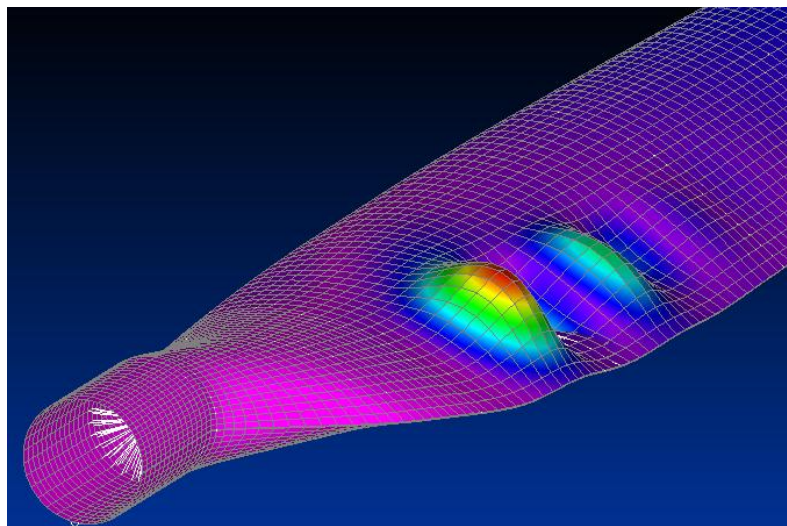


Figure 11: Close – up view of first buckling mode.

4.3 Turbine blade post buckling - numerical investigation and results

For the simulation of the damage it has been adopted the technique of reducing locally the material properties of some elements of the whole structure. In particular to the elements belonging to the first two sections the same material with lower mechanical properties has been attributed (Table 4).

	Longitudinal Young's modulus E_1 [GPa]	Transversal Young's modulus E_2 [GPa]	Shear modulus G_{12} [GPa]	Poisson's ratio ν	Mass density ρ [kg/m ³]
undamaged	30.0	7.0	4.0	0.22	2200
damaged	23.0	4.0	3.0	0.22	2200

Table 4: Mechanical properties of the undamaged and damaged models.

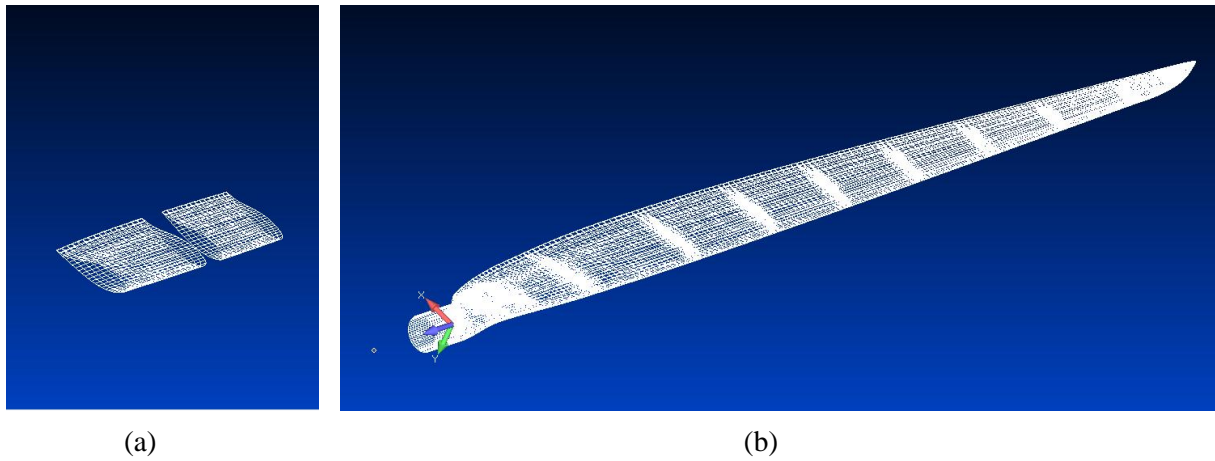


Figure 12: Isometric view of FE model: damage elements (a) and full wing blade turbine (b) elements.

Mode n.	Pre buckling		Post buckling	
	Numerical	Experimental	Numerical	Experimental
	Natural frequency [Hz]	Natural frequency [Hz]	Natural frequency [Hz]	Natural frequency [Hz]
1	3.921	4.005	3.2432	3.316
2	7.046	7.994	6.8395	6.457
3	12.064	11.376	11.907	10.049
4	24.305	24.887	22.776	22.964

Table 5: Comparison of the numerical and experimental natural frequencies pre and post buckling of the investigated blade.

5 Vibration and aeroelastic analysis - beam model

In this section vibration analysis of a rotating beam and aeroelastic analysis are performed in order to determine normal modes and the shift of the natural frequencies with differential stiffness at different speed. For reason of simplicity and in view to reduce the computation cost, it is common practice to model wind turbine components as beam structures.

Therefore, the complex 3D full blade model is converted into a simplified equivalent beam model of 1D type with missing shape data. The beam model was modelled first with a uniform section and then with more detailed sections. In order to verify the reliability of the beam model, a static analysis was performed

for both the 3D full blade model and for the beam model; the same load first and moment later was applied to the models' tip and the maximum deformation and rotation was evaluated. From the results it can be seen that the beam model matches the 3D full model and so it can be used to perform vibro-aeroelastic analysis.

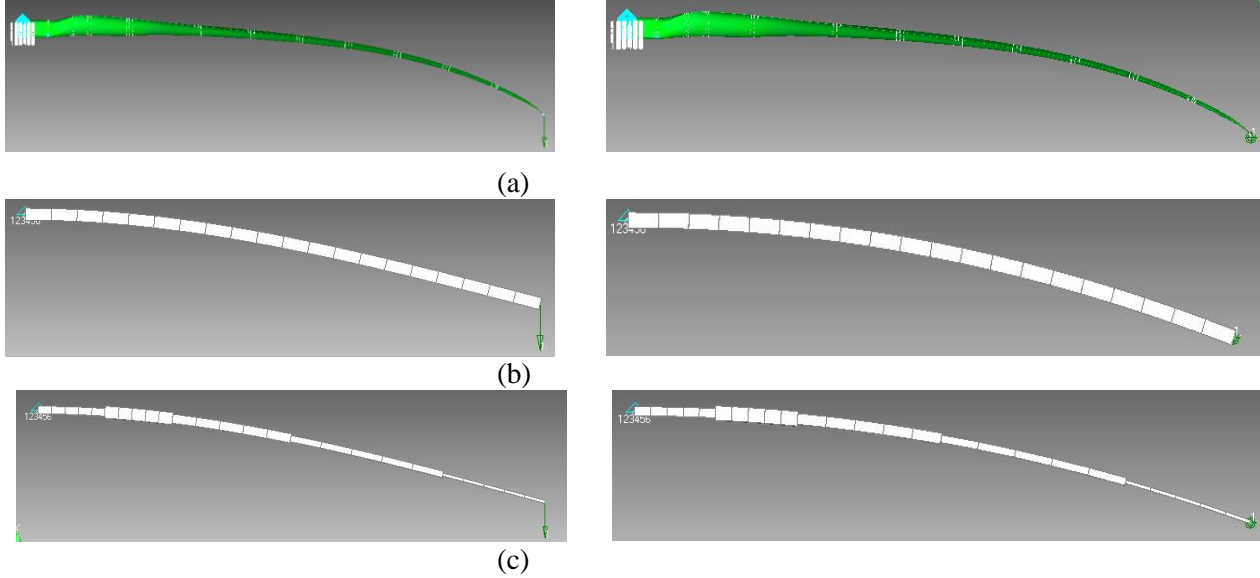


Figure 13: 3D full blade model (a) and beam model with regular section (b) and not-regular section (c).

5.1 Vibration investigation of the blade free to move

Numerical investigation of the effect of the rotational velocity of the blade on the natural frequencies was performed. The model was prepared by using the commercial software Femap for a linear static analysis and an input bulk data file was compiled. The bulk data file was manually modified to perform the normal mode analysis with the calculated differential stiffness by adding a new subcase with the STATSUB command. In Table 6 the first five natural frequencies for different rotational speed are reported. From the results it is possible to highlight the increase of the natural frequencies with increasing speed. The variation of the natural frequencies with rotational speed is more evident in Figure 14. As it can be note from the results it seems that there is almost an inversion of the fourth and fifth modes at $\Omega=180$ rpm. Again it can be note that the natural frequencies at $\Omega=0$ are not the same ones obtained for the full blade model, but they are really close. This difference can be reduced adopting a not uniform distribution of the mass along the beam.

#	Frequency [Hz]					
	$\Omega=0$ [rpm]	$\Omega=5$ [rpm]	$\Omega=10$ [rpm]	$\Omega=30$ [rpm]	$\Omega=50$ [rpm]	$\Omega=100$ [rpm]
1	0.5106	0.5179	0.5417	0.7455	1.0305	1.8401
2	2.0326	2.0344	2.0406	2.1043	2.2244	2.7232
3	3.1846	3.1910	3.2123	3.4280	3.8178	5.2926
4	8.8672	8.8735	8.8945	9.1120	9.5250	11.271
5	12.335	12.336	12.341	12.399	12.511	13.035

Table 6: Numerical natural frequencies of the blade modelled as beam at different rotational velocity.

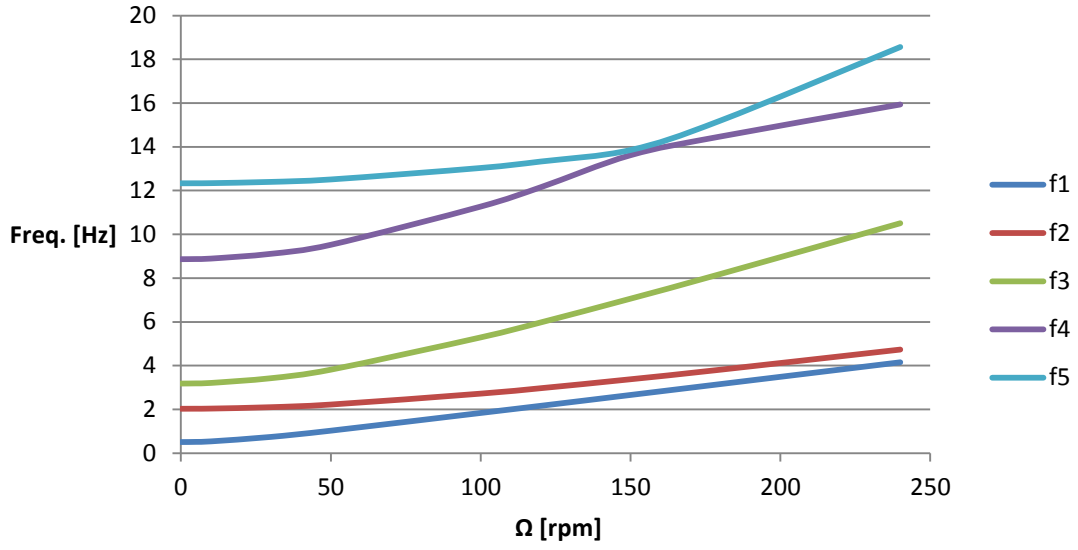


Figure 14: Variation of natural frequencies at different rotational velocities.

5.2 Aeroelastic investigation

The increased flexibility of wind turbine blades justifies the need for considering aeroelastic effects for the design of novel thinner blade sections. This paragraph presents an approach for aeroelastic calculation based on classical method employed for aircraft surfaces including the centrifugal stiffness induced by the rotational speed. In this preliminary aeroelastic calculations some simplification are considered. They relate mainly to assume a rigid tower and a spanwise averaged wind speed. First hypothesis allows avoiding the whirl flutter problem, which is outside the interest of this paper. The second hypothesis is required by the selected method which, coming from airplane aeroelastic calculations, does not allow a spanwise variable wind speed.

The equations of motion of a rotating beam, considering rotational stiffening effect, [4-8], are:

$$[M_S]\{\ddot{x}\} + [C_S]\{\dot{x}\} + ([K_S] + [K_G(\Omega)])\{x\} = [M_A]\{\ddot{\alpha}\} + [C_A]\{\dot{\alpha}\} + [K_A]\{\alpha\} \quad (8)$$

where the matrices subscripted S (structural) and A (aerodynamic) are composed of elemental mass, damping and stiffness terms and the stiffness matrix subscripted G stands for the centrifugal stiffening contribution due to the rotational speed.

This equation allows the use of a standard aeroelastic solution as implemented inside commercial software, like MSC/Nastran, provided the addition of the centrifugal stiffness $[K_G]$. This matrix can be computed separately and properly added to the structural stiffness matrix before the aeroelastic computation. This operation is allowed to the user of the aeroelastic solution using the ALTER options described in [8].

The procedure starts computing the $[K_S] + [K_G(\Omega)]$ matrices from a static case of the blade model loaded by the centrifugal forces proportional to the rotational speed Ω . The stiffness matrices are then stored for being recalled by the aeroelastic solution. These matrices replace the stiffness matrix computed by the program before the computation of the aeroelastic effect. This approach is not automatic because it requires two separate steps, but when implemented, it results in a not complex tool.

The validity of the approach has been firstly checked for structural dynamics computation, calculating the variation of the frequencies (mode-shapes are generally not affected, for simple structures) due to rotational speed Ω . The case presented here has specifically selected for highlighting the aeroelastic

problem of a rotating beam. The following table and relative figure show how the first three frequencies are affected by the stiffening of the centrifugal forces:

#	Frequency [Hz]			
	$\Omega=0$	$\Omega=5$	$\Omega=10$	$\Omega=30$
1	1.96	5.49	17.39	32.65
2	8.75	11.70	20.48	76.94
3	17.76	20.48	37.56	101.78

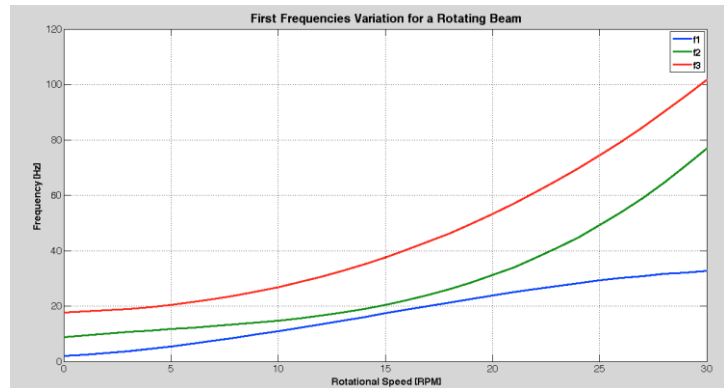
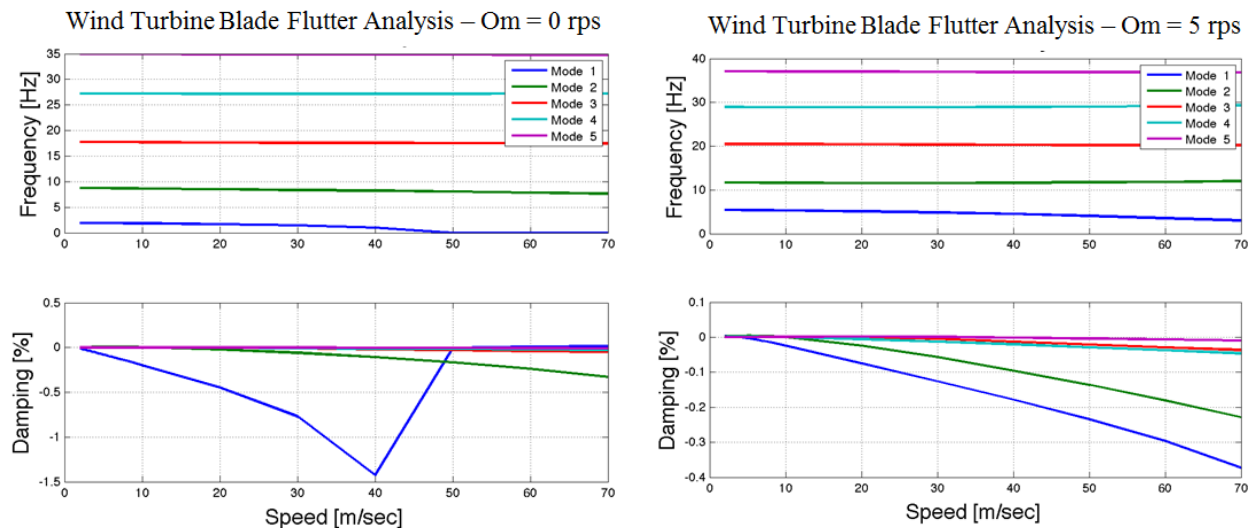


Figure 15: Stiffening effect of the centrifugal forces on the first frequencies of a cantilever rotating beam.

Once the updated stiffness matrix is available, the aeroelastic calculation can be pursued both for the static (load distribution on a flexible blade) and dynamic (flutter and dynamic response) case. Here some example for the flutter calculation have been carried out and reported in Figure 16. It is interesting to note from these plots that changing the rotational speed, may significantly vary the aeroelastic behaviour of the wind turbine blade, passing from the evidence of a static divergence ($= 0$ rps) to the absence of any aeroelastic instability ($= 5$ rps), to another divergence case at smaller speed than previously computed ($= 15$ rps) to a classical flutter ($= 30$ rps). It should be remembered that, as usually assumed, the structural damping characteristics is supposed to be zero for obtaining conservative results, but in any case, it turns out that considering the aeroelastic effect may be important for the SHM of flexible wind turbine blade.



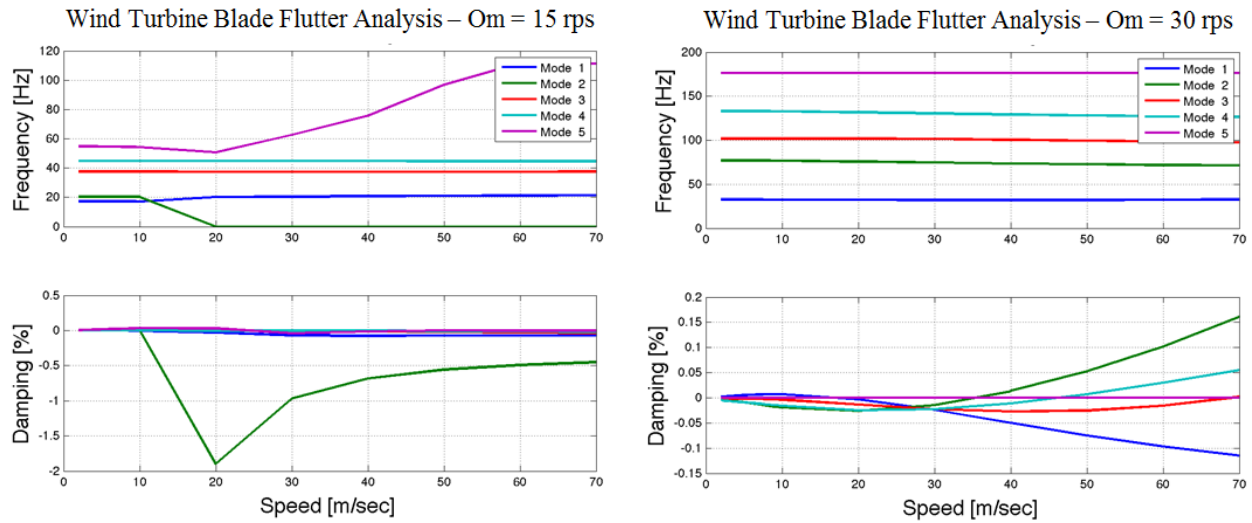


Figure 16 - V-g-f Plots of a wind turbine blade at different rotational speed.

6 Conclusions

In recent years, stability problems in wind turbine structures have obtained increasing attention due to the trend towards larger and more flexible structures. A well-known example of a stability problem, that eventually might lead to failure of the whole structure, is the occurrence of dynamic unstable edgewise vibrations. For aerodynamic loading in general, and for dynamic stability problems in particular, the deflection patterns of the wind turbine blades are of vital importance.

The present investigation has demonstrated that the structural integrity of a structure can be monitored by using modal parameters, like natural frequencies, damping characteristics and mode shapes. Operational modal analysis was performed and results were compared with numerical ones and good correlation between them has been found. Furthermore, in order to take into account the influence of the centrifugal stiffness induced by rotational speed on vibration and aeroelastic behavior of the blade, a numerical analysis on the beam model was performed by using a particular subcase in Nastran. From the results it can be noted that changing the rotational speed, may significantly vary the aeroelastic behavior of the wind turbine blade.

Acknowledgements

The authors would like to thank the staff of the EolPower Group, a spin-off of the Industrial Engineering Department at the University of Naples Federico II, and Wind4Life srl for providing us the wind turbine and for the assistance during the experimental tests.

References

- [1] G.H. James III, T.G. Carne, J.P. Lauffer, *The Natural Excitation Technique (NExT) for Modal Parameter Extraction From Operating Wind Turbines*, Sandia National Laboratories technical report, USA, February 1993.
- [2] B. Peeteers, P. Guillaume, H. Van der Auweraer, B. Cauberghe, P. Verboven, and J. Leuridan, *The PolyMAX frequency-domain method: a new standard for modal parameter estimation?*, Shock and Vibration, 11:395-409, 2004

- [3] B. Peeters, H. Van der Auweraer, F. Vanhollenbeke, P. Guillaume, *Operational modal analysis for estimating the dynamic properties of a stadium structure during a football game*, Shock and Vibration, 14(4):283-303, 2007.
- [4] E. Kosko, *The Free Uncoupled Vibrations of a Uniformly Rotating Beam*, Institute of Aerophysics, University of Toronto, March 1960
- [5] R.L. Bielawa, *Rotary Wing Structural Dynamics and Aeroelasticity*, AIAA Educational Series, 1992
- [6] D.A. Spera, ed., *Collected Papers on Wind Turbine Technology*, NASA CR-195432, May 1995
- [7] W.P. Rodden, *MSC/Nastran Handbook for Aeroelastic Analysis*, The MacNeal schwendler Corp., Report MSR-57, 1987
- [8] M. Reymond, ed., *DMAP Programmer's Guide*, MSC Software Doc 10013, 2013